Nonlinear fiber optics: its history and recent progress [Invited]

Govind P. Agrawal

The Institute of Optics, University of Rochester, Rochester, New York 14627, USA (gpa@optics.rochester.edu)

Received August 25, 2011; accepted September 21, 2011;
posted October 6, 2011 (Doc. ID 153523); published November 11, 2011

This review begins with an historical introduction to the field of *nonlinear fiber optics* and then focuses on the propagation of short optical pulses inside optical fibers. The underlying nonlinear Schrödinger equation is used to discuss the nonlinear phenomenon of self-phase modulation that leads to the formation of solitons in the presence of anomalous dispersion. Recent work on supercontinuum generation is reviewed with emphasis on the important nonlinear processes, such as the fission of higher-order solitons and intrapulse Raman scattering. Applications of fiber-based supercontinuum sources are also discussed in diverse areas ranging from biomedical imaging to frequency metrology. The last part describes applications resulting from nonlinear phenomena, such as cross-phase modulation, stimulated Raman scattering, and four-wave mixing.

OCIS codes: 190.4370, 130.4310.

1. HISTORICAL INTRODUCTION

The advent of the laser [1] in 1960 gave birth to a new field of optics. It was called *nonlinear optics* because the response of atoms to an intense electromagnetic fields could no longer be taken to be linear in the electric field. The observation of second harmonic generation [2] in 1961 was soon followed with the discovery of a large number of nonlinear processes, including stimulated Raman scattering (SRS) [3], intensity-dependent refractive index [4], stimulated Brillouin scattering (SBS) [5], and four-wave mixing (FWM) [6]. The decade of 1960s also saw rapid theoretical advances that led to a good understanding of the observed experimental results [7].

Optical fibers that were available during the 1960s exhibited very high losses. Since silica glass does not exhibit a high nonlinearity, there was little incentive for considering optical fibers for nonlinear-optics experiments. The situation changed in 1970 when scientists working at Corning were first able to reduce losses of optical fibers dramatically [8]. Soon after, Stolen's group at Bell Laboratories used silica fibers for demonstrating a variety of nonlinear effects, including SBS and SRS, self-phase modulation (SPM), the Kerr effect, and FWM [9–14]. This work was followed with the discovery of solitons in optical fibers [15–17], and it eventually gave birth to a new branch of nonlinear optics that became an active area of research during the 1980s. For a more detailed history of the early years of this field, the reader is referred to a 2008 article by Stolen [18]. I became involved in this area around 1984 and published a book in 1989 with the title *Nonlinear Fiber Optics* [19]. Since then, the field of nonlinear fiber optics has grown considerably, especially after the advent of photonic-crystal and other microstructured fibers. My book has grown with it, and its fifth edition will appear in 2012. This overview is intended to summarize the current status of the field of nonlinear fiber optics together with some indication of future directions.

2. BASIC FEATURES OF OPTICAL FIBERS

The new feature of optical fibers compared with nonlinear liquids and crystals is that any light launched into them remains confined to the core of the fiber, thanks to the dielectric waveguiding provided by the refractive-index difference between its core and cladding. In the case of single-mode fibers, the core diameter is $<10\,\mu$m and can be reduced to below $1\,\mu$m in modern microstructured fibers. The other feature of optical fibers that becomes critically important is chromatic dispersion, resulting in a frequency dependence of the refractive index. In this section I discuss how these features of optical fibers affect nonlinear optical phenomena.

A. Why Use Fibers for Nonlinear Optics?

The first question one may ask is why bother to use fibers for nonlinear optics. As far as nonlinear materials go, silica glass is not known for its nonlinear properties. The second-order susceptibility vanishes for this glass because SiO_2 exhibits inversion symmetry. Thus, most nonlinear effects stem from its third-order susceptibility, whose value for silica glass is smaller by a factor of 100 or more compared to many crystals and liquids [20]. Similarly, the measurements of Raman- and Brillouin-gain coefficients in silica fibers show that their values are smaller by 2 orders of magnitude or more compared with other common nonlinear media.

The answer to this riddle lies in the relatively long lengths over which fibers can maintain high optical intensities. In spite of intrinsically small values of the nonlinear coefficients, nonlinear effects in optical fibers can be observed at relatively low power levels. This is possible because of two important characteristics of single-mode fibers—a small spot size (mode diameter $<10\,\mu$m) and extremely low losses (<1 dB/km) in the wavelength range of $1.0–1.6\,\mu$m.

A figure of merit for judging the efficiency of a nonlinear process in bulk media is the product $I_0 L_{\text{eff}}$, where I_0 is the

optical intensity and $L_{\rm eff}$ is the effective length of the region where such a high intensity can be maintained [21]. If light is focused to a spot of radius w_0, then $I_0 = P_0/(\pi w_0^2)$, where P_0 is the incident optical power. Clearly, I_0 can be increased by focusing the light tightly to reduce w_0. However, this results in a smaller $L_{\rm eff}$ because the length of the focal region decreases with tight focusing. For a Gaussian beam, $L_{\rm eff} \sim \pi w_0^2/\lambda$, and the product

$$(I_0 L_{\rm eff})_{\rm bulk} = \left(\frac{P_0}{\pi w_0^2}\right)\frac{\pi w_0^2}{\lambda} = \frac{P_0}{\lambda} \tag{1}$$

is independent of the spot size w_0.

In a single-mode fiber, the spot size w_0 is set by the core diameter and the refractive-index difference between its core and cladding. The important point is that the same spot size can be maintained across its entire length L. In this case, the interaction length $L_{\rm eff}$ is limited by the fiber loss α. Using $I(z) = I_0 \exp(-\alpha z)$, where $I_0 = P_0/(\pi w_0^2)$ and P_0 is the optical power coupled into the fiber, the product $I_0 L_{\rm eff}$ becomes

$$(I_0 L_{\rm eff})_{\rm fiber} = \int_0^L I_0 e^{-\alpha z}\,{\rm d}z = \frac{P_0}{\pi w_0^2 \alpha}(1 - e^{-\alpha L}). \tag{2}$$

A comparison of Eqs. (1) and (2) shows that, for sufficiently long fibers, the efficiency of a nonlinear process in optical fibers can be improved by a factor

$$\frac{(I_0 L_{\rm eff})_{\rm fiber}}{(I_0 L_{\rm eff})_{\rm bulk}} = \frac{\lambda}{\pi w_0^2 \alpha}, \tag{3}$$

where $\alpha L \gg 1$ was assumed. In the visible region, the enhancement factor is $\sim 10^7$ for $\lambda = 0.53\,\mu$m, $w_0 = 2\,\mu$m, and $\alpha = 2.5 \times 10^{-5}\,{\rm cm}^{-1}$ (10 dB/km). In the wavelength region near $1.55\,\mu$m ($\alpha = 0.2$ dB/km), the enhancement factor can approach 10^9. It is this tremendous enhancement in the efficiency of the nonlinear processes that makes silica fibers a suitable nonlinear medium for the observation of a wide variety of nonlinear effects at relatively low power levels.

B. Pulse Propagation Through Optical Fibers

Although continuous-wave (CW) fields are sometimes used, especially in the context of SBS, SRS, and FWM, this review does not focus on them. Rather, we ask how short optical pulses are affected by the nonlinear effects during their propagation inside optical fibers. As such pulses are also affected by the dispersive effects simultaneously, the combination of the dispersive and nonlinear effects gives rise to a variety of novel phenomena. Two examples are provided by soliton formation and supercontinuum generation. To understand them, we need to first solve Maxwell's equations inside a dispersive nonlinear medium. Since details are available elsewhere [19], only the main steps are summarized here.

Consider the simplest situation in which a single input pulse at the carrier frequency ω_0 is launched such that it excites a single mode of the fiber. If we assume that the pulse maintains its linear polarization along the x axis during propagation inside the fiber along its length (the z axis), the electric field can be written in the form

$$\mathbf{E}(\boldsymbol{r}, t) = \frac{1}{2\pi}\int_{-\infty}^{\infty} \hat{x} F(x, y, \omega)\bar{a}(0, \omega) e^{i[\beta(\omega)z - \omega t]}\,{\rm d}\omega, \tag{4}$$

where $\hat{x}$ is a unit vector along the x axis and $F(x, y, \omega)$ represents the spatial distribution of the fiber. The physical meaning of this equation is clear. Each spectral component of the input field propagates as a plane wave and acquires a slightly different phase shift because of the frequency dependence of the propagation constant $\beta(\omega)$.

As an exact functional form of $\beta(\omega)$ is rarely known, it is useful to expand it in a Taylor series around the carrier frequency ω_0 as

$$\beta(\omega) = \beta_0 + (\omega - \omega_0)\beta_1 + \frac{1}{2}(\omega - \omega_0)^2\beta_2 + \ldots, \tag{5}$$

where various dispersion parameters are defined as $\beta_m = (d^m\beta/d\omega^m)_{\omega} = \omega_0$. Depending on the pulse bandwidth, one can stop after the second-order dispersion term containing β_2 or may need to include the third- and higher-order dispersion terms. Another common approximation replaces $F(x, y, \omega)$ with its value at the carrier frequency ω_0. It is also useful to remove the rapidly varying part of the optical field at this frequency and introduce a slowly varying pulse envelope $A(z, t)$ by writing Eq. (4) in the form

$$\mathbf{E}(\boldsymbol{r}, t) = \hat{x} F(x, y, \omega_0) A(z, t) e^{i(\beta_0 z - \omega_0 t)}. \tag{6}$$

Maxwell's equations are then used to derive an equation for $A(z, t)$.

As outlined in [19], if we include both the Kerr and Raman contributions to the nonlinear polarization induced by light, the slowly varying pulse envelope $A(z, t)$ satisfies the following time-domain propagation equation:

$$\frac{\partial A}{\partial z} + \frac{\alpha}{2}A = i\sum_{m=1}^{\infty}\frac{i^m\beta_m}{m!}\frac{\partial^m A}{\partial t^m} + i\gamma\left(1 + \frac{i}{\omega_0}\frac{\partial}{\partial t}\right) \times \left(A(z, t)\int_0^{\infty} R(t')|A(z, t - t')|^2\,{\rm d}t'\right), \tag{7}$$

where α accounts for fiber losses and the nonlinear parameter γ is defined as

$$\gamma = \frac{\omega_0 n_2(\omega_0)}{c A_{\rm eff}}, \qquad A_{\rm eff} = \frac{\left[\iint |F(x, y, \omega_0)|^2\,{\rm d}x\,{\rm d}y\right]^2}{\iint |F(x, y, \omega_0)|^4\,{\rm d}x\,{\rm d}y}. \tag{8}$$

$A_{\rm eff}$ is known as the effective mode area that depends on how far the optical mode extends beyond the core region of the fiber. In obtaining this result, we neglected the dispersion of the Kerr parameter n_2. In the case of supercontinuum generation, it may become necessary to account for the frequency dependence of both $n_2(\omega)$ and $F(x, y, \omega)$. The reader is referred to [19] for further details.

The nonlinear response function $R(t)$ in Eq. (7) should include both the electronic and nuclear (Raman) contributions. Assuming that the electronic contribution is nearly instantaneous, the functional form of $R(t)$ can be written as

$$R(t) = (1 - f_R)\delta(t) + f_R h_R(t). \tag{9}$$

Both the Raman response function $h_R(t)$ and its fractional contribution $f_R \approx 0.18$ are known for silica [22]. Because of the amorphous nature of silica glasses, the Raman gain spectrum $g_R(\omega)$ of optical fibers, shown in Fig. 1(a), extends over a range >50 THz. Since $g_R(\omega)$ is related to the imaginary part of the Fourier transform of $h_R(t)$, it can be used to deduce its real part through the Kramers–Kronig relation. The inverse Fourier transform of $\tilde{h}_R(\omega)$ then provides the Raman response function $h_R(t)$ shown in Fig. 1(b).

C. Nonlinear Schrödinger Equation

Although Eq. (7) must be solved for ultrashort optical pulses, it can be simplified considerably for picosecond pulses, a common situation in many applications. To understand why that is so, we note from Fig. 1 that $h_R(t)$ has an appreciable magnitude only for $t < 1$ ps. Because of its compact nature, it can be replaced with a delta function $\delta(t)$ for pulses wider than 5 ps or so. At the same time, dispersive effects higher than second order can be ignored for such pulses. Using these two approximations, Eq. (7) is reduced to the following much simpler equation:

$$\frac{\partial A}{\partial z} + \frac{\alpha}{2}A + \beta_1 \frac{\partial A}{\partial t} + \frac{i\beta_2}{2}\frac{\partial^2 A}{\partial t^2} = i\gamma|A|^2 A. \tag{10}$$

One more simplification can be made. We can remove the β_1 term by using a frame of reference moving with the pulse at the group velocity $v_g = 1/\beta_1$ (the so-called retarded frame). After the transformation $T = t - \beta_1 z$, Eq. (10) takes the form

$$i\frac{\partial A}{\partial z} + \frac{i\alpha}{2}A - \frac{\beta_2}{2}\frac{\partial^2 A}{\partial T^2} + \gamma|A|^2 A = 0. \tag{11}$$

In the special case of $\alpha = 0$, Eq. (11) is referred to as the nonlinear Schrödinger (NLS) equation. One can justify neglecting the loss term for fibers shorter than 1 km, especially in the wavelength region near 1550 nm where losses are the smallest.

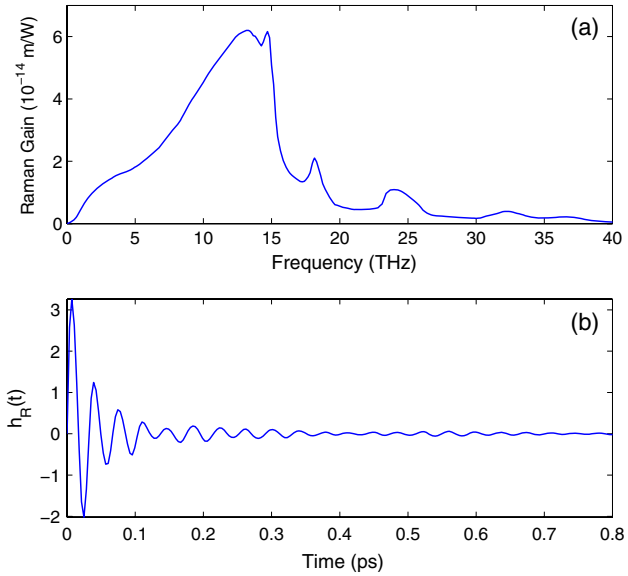

Fig. 1. (Color online) (a) Measured Raman gain spectrum of silica fibers [22]. (b) Temporal form of the Raman response function deduced from the gain data.

The NLS equation is a fundamental equation of nonlinear science and has been studied extensively in the context of solitons [19]. In the case of optical fibers, it involves two parameters, β_2 and γ, that govern the dispersive and nonlinear effects, respectively. The dispersion parameter β_2 can be positive or negative with values in the range of 0.1–20 ps^2/km, depending on how close the pulse wavelength is to the zero-dispersion wavelength of the fiber. The nonlinear parameter γ is positive and has a value in the range of 1–10 W^{-1}/km for most silica fibers; its values can be increased to beyond 100 W^{-1}/km in narrow-core photonic-crystal fibers (PCFs); even values >1000 W^{-1}/km have been realized using nonsilica glasses.

One can neglect fiber losses ($\alpha = 0$) for short fibers and normalize the NLS Eq. (11) using new variables defined as

$$U = \frac{A}{\sqrt{P_0}}, \qquad \xi = \frac{z}{L_D}, \qquad \tau = \frac{T}{T_0}, \tag{12}$$

where T_0 is the width of the incident pulse, P_0 is its peak power, and $L_D = T_0^2/|\beta_2|$ is called the dispersion length. The resulting NLS equation has the form

$$i\frac{\partial U}{\partial \xi} - \frac{\delta_2}{2}\frac{\partial^2 U}{\partial \tau^2} + N^2|U|^2 U = 0, \tag{13}$$

where $\delta_2 = \text{sgn}(\beta_2) = \pm 1$ and the parameter N is defined as

$$N^2 = \frac{L_D}{L_{\text{NL}}} = \frac{\gamma P_0 T_0^2}{|\beta_2|}. \tag{14}$$

The nonlinear length is defined as $L_{\text{NL}} = (\gamma P_0)^{-1}$. These two length scales govern pulse evolution in optical fibers. The single parameter N appearing in Eq. (13) can also be eliminated by introducing $u = NU$ [19].

3. SPM AND SOLITON FORMATION

A. Nondispersive SPM

Before considering solutions of the NLS equation, we first focus on a special case in which the dispersive term can be neglected in Eq. (11). This can occur when the length of fiber is much shorter than the dispersion length. For example, if $|\beta_2| = 1\ \text{ps}^2$/km and $T_0 = 10$ ps, the dispersion length is 100 km. If such a pulse is transmitted through a 1-km-long fiber, one can neglect the effects of dispersion in Eq. (11) by setting $\beta_2 = 0$. The resulting equation can be solved analytically by using $A = \sqrt{P}\exp(i\phi)$ and equating its real and imaginary parts, resulting in the following two equations for the power $P(z,T)$ and phase $\phi(z,T)$ of the pulse:

$$\frac{\partial P}{\partial z} = -\frac{\alpha}{2}P, \qquad \frac{\partial \phi}{\partial z} = \gamma P. \tag{15}$$

These equations are easily solved to obtain the power and phase of a pulse after it has propagated through a fiber of length L. The result is given by

$$P(z,T) = P(0,T)e^{-\alpha z}, \qquad \phi(L,T) = \phi(0,T) + \gamma P(0,T)L_{\text{eff}}, \tag{16}$$

where the effective length L_{eff} of a fiber of length L is defined as $L_{\text{eff}} = [1 - \exp(-\alpha L)]/\alpha$.

As expected, the power is reduced exponentially because of fiber losses. The important point is that, because of the nonlinear term, the pulse modifies its own phase. This nonlinear effect is known as SPM. Using $P(0,T) = P_0 f_p(T)$, where P_0 is the peak power of a pulse with shape governed by $f_p(T)$, the nonlinear phase shift resulting from SPM can be written as [19]

$$\phi_{\text{NL}}(L,T) = f_P(T)(L_{\text{eff}}/L_{\text{NL}}). \tag{17}$$

In the case of a CW beam, the input power is constant with $f_p(T) = 1$, and the nonlinear phase shift is time independent. However, it varies with time in the case of optical pulses and has the same temporal profile as the pulse shape.

Spectral changes induced by SPM are a direct consequence of the time dependence of ϕ_{NL}. This can be understood by recalling that a temporally varying phase implies that the instantaneous optical frequency differs across the pulse from its central value ω_0. The difference $\delta\omega$ is given by

$$\delta\omega(T) = -\frac{\partial \phi_{\text{NL}}}{\partial T} = -\left(\frac{L_{\text{eff}}}{L_{\text{NL}}}\right)\frac{\partial f_p}{\partial T}. \tag{18}$$

The time dependence of $\delta\omega$ is referred to as frequency chirping. The chirp induced by SPM increases in magnitude with the propagated distance. In other words, new frequency components are generated continuously as the pulse propagates down the fiber. These SPM-generated frequency components broaden the spectrum over its initial width at $z = 0$ for initially unchirped pulses. As an example, Fig. 2 shows how the pulse spectrum, obtained by taking the Fourier transform of $A(z,T)$, evolves along the fiber for a Gaussian pulse using $f_p(T) = \exp[-(T/T_0)^2]$ and $L_{\text{NL}} = 1\,\text{m}$. Several features are noteworthy. First, the spectrum broadens continuously along the fiber and develops sidebands on both sides of the original spectrum. The reason is that the SPM-induced chirp in Eq. (18) is negative near the leading edge (resulting in a redshift) and becomes positive near the trailing edge (a blueshift) of the pulse. Second, the sidebands at the two edges are most intense in the case of a Gaussian pulse. It is important to emphasize that SPM-induced spectral broadening depends considerably on both the shape and chirp of input pulses.

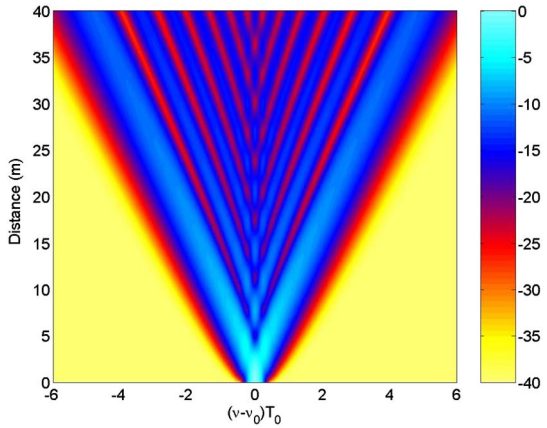

Fig. 2. (Color online) SPM-induced spectral broadening of a Gaussian along the length of a fiber for $L_{\text{NL}} = 1\,\text{m}$. The color scale represents the spectral density on a 40 dB scale (see the color bar).

However, the pulse shape does not change on propagation in the absence of dispersion.

B. Optical Solitons

The situation changes drastically when dispersive effects cannot be ignored inside the fiber. In general, both the pulse shape and spectrum change as the pulse propagates through the fiber. In the case of normal dispersion ($\beta_2 > 0$), optical pulses broaden with propagation. However, an interesting situation occurs in the case of anomalous dispersion ($\beta_2 < 0$). In this case, the pulse can form an optical soliton that evolves without any change in its shape and spectrum, provided the input pulse has a specific shape and a specific energy.

To understand soliton formation, we set $\delta_2 = -1$ ($\beta_2 < 0$) in Eq. (13) to ensure anomalous dispersion. This NLS equation belongs to a special class of equations that can be solved with the inverse scattering method [19]. The most dramatic result is that, when $N = 1$, the NLS Eq. (13) has a solution in the form

$$U(\xi,\tau) = \eta \,\text{sech}(\eta\tau)\exp(i\eta^2\xi/2), \tag{19}$$

where the arbitrary parameter η determines not only the soliton amplitude but also its width. This solution represents a fundamental soliton. In real units, the soliton width changes with η as T_0/η, i.e., it scales inversely with the soliton amplitude. This inverse relationship between the amplitude and the width of a soliton is the most crucial property of fundamental solitons.

The canonical form of the fundamental soliton is obtained by choosing $\eta = 1$ such that the input field $U(0,\tau) = \text{sech}(\tau)$. In this case, the pulse evolves as $U(\xi,\tau) = \text{sech}(\tau)\exp(i\xi/2)$. Since only the pulse phase is affected during propagation, neither the shape nor the spectrum of such input pulses change inside the fiber, a really remarkable result. One can verify by direct substitution in Eq. (13) that this solution is indeed a solution of the NLS equation. The peak power P_0 required to form a fundamental soliton is obtained from Eq. (14) by setting $N = 1$ and is given by $P_0 = |\beta_2|/(\gamma T_0^2)$. Using typical parameter values for dispersion-shifted fibers near the $1.55\,\mu\text{m}$ wavelength, $\beta_2 = -1\,\text{ps}^2/\text{km}$ and $\gamma = 3\,\text{W}^{-1}/\text{km}$, we find that P_0 is $\sim$1 W for $T_0 = 1\,\text{ps}$ but reduces to only 10 mW when $T_0 = 10\,\text{ps}$ because of its T_0^{-2} dependence. Thus, fundamental solitons can form in optical fibers at power levels available from semiconductor lasers.

A natural question is what happens if the initial pulse shape or the peak power is not matched precisely, and the input pulse does not form an optical soliton right away. The effect of pulse shape on soliton formation can be investigated by solving Eq. (13) numerically. It turns out that, as long as N is close to 1 and the pulse is bell shaped, the pulse adjusts its shape and width and evolves asymptotically into a fundamental soliton with the correct "sech" shape [19]. The reason is that, similar to spatial modes of an optical fiber, a fundamental soliton represents a temporal mode of a nonlinear waveguide. In general, fundamental solitons form for values of N in the range $0.5 < N < 1.5$. It is this relative insensitivity to the exact values of input parameters that makes the use of solitons feasible in practical applications. However, it is important to realize that, when input parameters deviate substantially from their ideal values, a part of the pulse energy is invariably shed away in the form of dispersive waves.

One may ask what happens for $N > 1.5$. The answer is provided by the inverse scattering method in terms of higher-order solitons [19] that form for integer values of N. A higher-order soliton changes its shape and spectrum during propagation in a periodic fashion such that the input pulse is reproduced after each soliton period $\xi_p = \pi/2$. As an example, Fig. 3 shows the evolution of two higher-order solitons (for $N = 2$ and 4) over two soliton periods. When $N = 2$, the pulse first goes through a contraction phase, splits into two distinct pulses as it propagates down the fiber, and then merges again to recover the original shape at the end of a soliton period at $\xi = \pi/2$. This pattern is repeated over each fiber section of length $(\pi/2)L_D$. The evolution is much more complex for $N = 4$, but pulses undergo periodic splitting and recombining for any value of N. The pulse spectrum also changes and develops a multipeak structure at certain distances. As seen in the following section, higher-order solitons can be used to generate a supercontinuum, the name given to an unusually wide spectrum.

4. SUPERCONTINUUM GENERATION

When femtosecond pulses are launched into highly nonlinear fibers with large enough power that N is initially close to 10 or larger, their spectra undergo extreme broadening, resulting in an output spectrum that may extend over a range exceeding 100 THz. Such a spectrum is referred to as a supercontinuum and has found a variety of applications.

A. Fission of Higher-Order Solitons

As mentioned in Subsection 2.C, Eq. (11) is not applicable for femtosecond pulses, and we must resort to solving Eq. (7), often called the generalized NLS equation. It is common to approximate $h_R(t)$ in Fig. 1(b) with the following analytic form [19]:

$$h_a(t) = \frac{\tau_1^2 + \tau_2^2}{\tau_1 \tau_2^2} \exp(-t/\tau_2) \sin(t/\tau_1), \tag{20}$$

with $\tau_1 = 12.2$ fs and $\tau_2 = 32$ fs. One should be careful in using Eq. (20) because it approximates the actual Raman gain spectrum in Fig. 1(a) with a Lorentzian profile, and thus fails to reproduce the hump seen there at frequencies below 5 THz. A modified form of $h_R(t)$ was proposed in 2006 by Lin and Agrawal to address this issue [23]. It adds a second term such that

$$h_R(t) = (1 - f_b) h_a(t) + f_b h_b(t), \tag{21}$$

$$h_b(t) = (2\tau_b - t)\tau_b^{-2} \exp(-\tau/\tau_b), \tag{22}$$

with $f_R = 0.245, f_b = 0.21$, and $\tau_b = 96$ fs. The use of this new form improves numerical predictions considerably.

It is still useful to work in the soliton units introduced in Eq. (12). If we retain dispersion terms up to third order, Eq. (7) takes the following form:

$$i\frac{\partial U}{\partial \xi} - \frac{\delta_2}{2}\frac{\partial^2 U}{\partial \tau^2} + N^2|U|^2U = i\delta_3\frac{\partial^3 U}{\partial \tau^3} + iN^2\left(1 + is\frac{\partial}{\partial t}\right) \times \left(U(\xi,\tau)\int_0^\infty R(\tau')|U(\xi,\tau-\tau')|^2 d\tau'\right), \tag{23}$$

where the self-steepening parameter $s = (\omega_0 T_0)^{-1} \ll 1$ for pulses as short as 10 fs and can often be neglected in practice. The third-order dispersion (TOD) parameter, $\delta_3 = \beta_3/(6|\beta_2|T_0)$, plays an important role in the dynamics of femtosecond pulses and can be positive or negative. Even fourth- and higher-order dispersion terms are sometimes included. Equation (23) can be used to study propagation of femtosecond pulses in both the normal- and anomalous-dispersion regions and it reveals several new effects.

The phenomenon of soliton fission was predicted as well as observed during the 1980s [24–27]. It occurs whenever a higher-order soliton is perturbed inside an optical fiber by third- or higher-order dispersion. As an example, Fig. 4 shows the temporal and spectral evolution of a third-order soliton ($N = 3$) by using $\delta_2 = -1$ (anomalous dispersion) with $\delta_3 = 0.01$. The Raman contribution in Eq. (23) was neglected

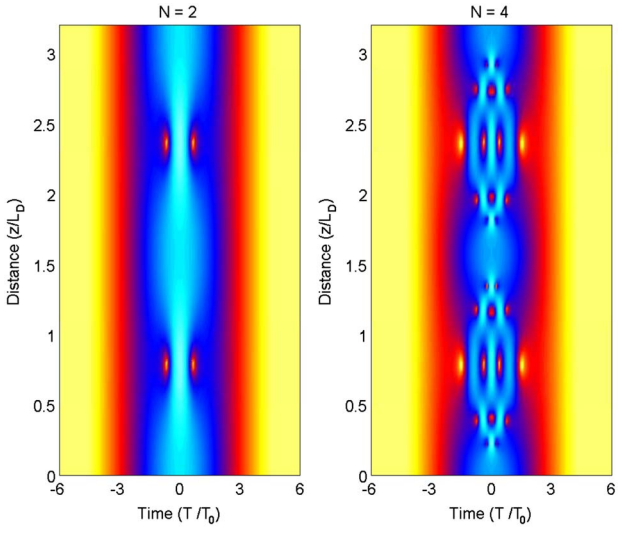

Fig. 3. (Color online) Evolution of second- and fourth-order solitons over two soliton periods. The 40 dB intensity scale is the same as in Fig. 2.

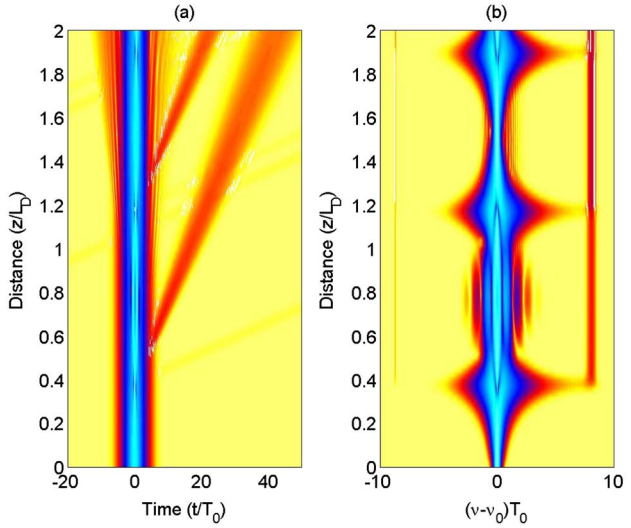

Fig. 4. (Color online) (a) Temporal and (b) spectral evolution of a third-order soliton ($N = 3$) over two dispersion lengths for $\delta_3 = 0.01$. The intensity scale is logarithmic as in Fig. 2. The diverging red regions in (a) represent dispersive waves at a frequency marked by the red vertical line in part (b).

to show that the fission process is dominated by the TOD in practice. Soliton fission breaks an Nth soliton into N fundamental solitons of different widths and peak powers given by [25]

$$T_k = \frac{T_0}{2N+1-2k}, \qquad P_k = \frac{(2N+1-2k)^2}{N^2} P_0, \tag{24}$$

where $k = 1$ to $\bar{N}$, where $\bar{N}$ is the integer closest to N when N is not an integer. The individual solitons are not apparent in Fig. 4(a) because they do not separate much from each other when Raman contribution is neglected. However, one sees a clear signature of soliton fission through the appearance of a new spectral peak in Fig. 4(b) at a distance of $\xi = 0.4$ (vertical red line). During the fission process, a part of the pulse energy is transferred to a dispersive wave at a frequency that satisfies a specific phase-matching condition [28]. The frequency is approximately given by $\omega_d = \omega_0 - 3\beta_2/\beta_3$ and it falls on the blue side of the original carrier frequency ω_0 of the incident pulse in Fig. 4(b). If the sign of δ_3 were reversed, it would fall on the red side of that frequency. In the time domain, a dispersive wave spreads with propagation and falls behind the main soliton because the two propagate at different speeds. This is clearly seen in Fig. 4(a).

B. Intrapulse Raman Scattering

Intrapulse Raman scattering has its origin in the Raman term in Eq. (23). Physically speaking, for short pulses with a relatively wide spectrum, the Raman gain can amplify the low-frequency components of a pulse by transferring energy from the high-frequency components of the same pulse. As a result, the pulse spectrum shifts continuously toward the red side as the pulse propagates through the fiber. Such a Raman-induced frequency shift (RIFS) is also known as the soliton self-frequency shift because it becomes relatively large for solitons that maintain their width during propagation inside a fiber. The RIFS was first observed in a 1986 experiment [29] and its Raman origin was also clarified at that time [30]. A more general theory was developed later [31]. Much larger values of the RIFS (> 50 THz) were observed after 2000 with the advent of microstructured fibers [32].

To see how intrapulse Raman scattering affects a higher-order soliton, one should solve Eq. (23) numerically. As an example, Fig. 5 shows the temporal and spectral evolution of a fourth-order soliton ($N = 4$) by using $\delta_2 = -1$, $\delta_3 = 0.02$, and $s = 0.01$. The input pulse is of the form $U(0,\tau) = \mathrm{sech}(\tau)$. A comparison of Figs. 4 and 5 shows remarkable changes occurring when intrapulse Raman scattering is included. In particular, notice the temporal pattern and a substantial broadening of the spectrum.

We can understand the evolution scenario seen in Fig. 5 as follows. The fourth-order solitons undergo fission at a distance near $\xi = 0.3$ and a dispersive wave is generated on the blue side of the original spectrum that falls behind the original because of its slower speed (similar to the $N = 3$ case seen in Fig. 4). The new feature in Fig. 5(a) is the resulting four fundamental solitons separate from each other as their trajectories bend to the right by different amounts. This is a consequence of the RIFS induced by intrapulse Raman scattering. Since the RIFS is the largest for the shortest soliton, its spectrum shifts the most toward the red side in Fig. 5(b), and its position also shifts the most in Fig. 5(a). Bending of the soliton trajectory is due to a continuous shift of the soliton spectrum with propagation. Any change in the soliton's frequency is accompanied with a reduction in the soliton's speed because of dispersion. This deceleration appears as a bending of soliton trajectories in the time domain.

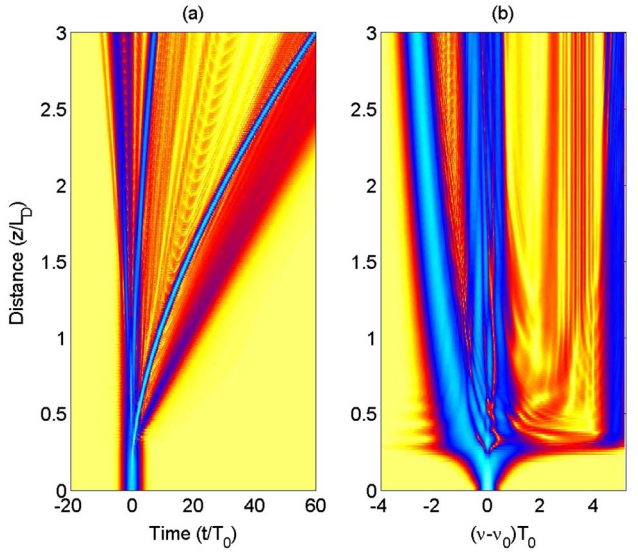

Fig. 5. (Color online) (a) Temporal and (b) spectral evolution of a $N = 4$ soliton over three dispersion lengths. The intensity scale is logarithmic as in Fig. 2. The tilted blue lines in (a) represent two fundamental solitons traveling slower than the input pulse because of a RIFS of their spectra in part (b).

The spectral broadening seen in Fig. 5 increases rapidly with increasing values of N. It turns out that the resulting supercontinuum can extend over a frequency range exceeding 100 THz when the soliton order associated with the input pulse exceeds 10 or so [33–36]. The next two subsections describe the recent experimental progress in this area and diverse applications of the resulting supercontinuum sources.

C. Recent Experimental Progress

In a 2000 experiment, 100 fs pulses with 7 kW peak power at 790 nm were launched in the anomalous-dispersion region of a microstructured fiber that was only 75 cm long [33]. Even for such a short fiber, the supercontinuum extended from 400 to 1600 nm and was also relatively flat over the entire bandwidth (on a logarithmic power scale). Similar features have been observed in many experiments using different types of fibers. An ultralarge bandwidth was realized in 2009 when a 2-cm-long fluoride fiber was pumped with 180 fs pulses at a wavelength of 1450 nm [35]. Figure 6(a) shows the output spectrum observed at a peak-power level of 50 mW. Numerical evolution of the supercontinuum over 2 cm is shown in Fig. 6(b) for a pulse with peak power of 0.4 MW. The supercontinuum even for such a short fiber extends from the ultraviolet to the infrared region (up to 6 μm).

Recent work has shown that a supercontinuum can form even when input pulses are launched in the normal-dispersion region of a suitably designed PCF [37]. The most important feature of such fibers was that femtosecond pulses launched into them did not spread too much in spite of experiencing normal dispersion. Figure 7(a) shows the broadband spectra observed at the output of a 50-cm-long PCF (fabricated with a 2.3-μm-diameter core) when it was pumped at a wavelength of

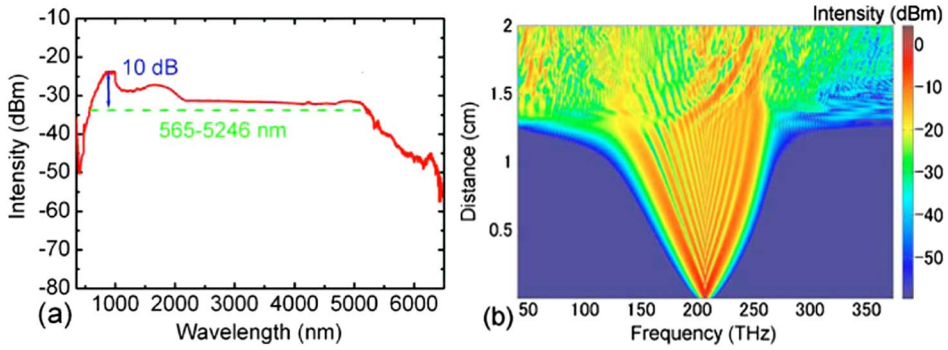

Fig. 6. (Color online) (a) Supercontinuum observed at the output of a 2-cm-long fluoride fiber pumped at 1450 nm with 180 fs pulses with 50 MW peak power. (b) Simulated evolution for a pulse launched with 0.4 MW peak power. (Reproduced with permission from [35], ©2009 American Institute of Physics.)

1050 nm with 50 fs pulses of energies ranging from 0.25 to 7.8 nJ. Figure 7(b) shows the output spectra when the same PCF was pumped at 790 nm. In both cases, the supercontinua extend over a bandwidth close to 800 nm at the highest pulse energy and are relatively flat and smooth compared to those formed in the anomalous-dispersion region. Moreover, they exhibit much better coherence properties.

Even CW lasers can be used for generating a supercontinuum [38]. The physical mechanism in the case of a CW input is the nonlinear phenomenon of modulation instability [19] that converts CW light into a train of short fundamental solitons whose widths vary over a wide range because of inherent noise [36]. Various fundamental solitons shift their spectra toward longer wavelengths through the RIFS process, similar to the case of femtosecond pulses discussed earlier. As they shift their spectra, solitons also slow down as long as they experience anomalous dispersion. As a result, they collide (overlap temporally) with neighboring solitons (or dispersive waves) and interact with them though cross-phase modulation (XPM). It turns out that such a collision transfers energy to the slowing soliton, which reduces its width (to maintain the condition $N = 1$) and slows down even more, and its spectrum shifts even further toward longer wavelengths. Multiple soliton collisions eventually produce a supercontinuum that is extended mostly toward the red side of the input wavelength.

By 2009, the use of a PCF whose core was both tapered and doped with GeO_2 created a CW supercontinuum that extended toward wavelengths as short as 450 nm [39]. Figure 8 compares the spectra obtained for uniform-core and tapered-core PCFs whose core was doped with GeO_2. In case (a) of a uniform-core PCF, the launched CW power at 1075 nm was 70 W, and the supercontinuum extended from 550 to >1750 nm with a spectral power variation of less than 12 dB. In case (b), a uniform-core section of 50 m was followed with a 130-m-long PCF section whose outer diameter decreased from 135 to 85 μm. When pumped with 40 W of CW power, the supercontinuum extended from 470 to >1750 nm and thus covered the entire visible region, as is also evident from the white spot in Fig. 8(c). When a prism was used to disperse the output light, a rainbowlike spectrum was observed, as seen in the inset of Fig. 8. These results clearly show that an ultrabroad supercontinuum covering both the visible and near-infrared regions can be produced with 1060 nm pumping provided the PCF is suitably designed.

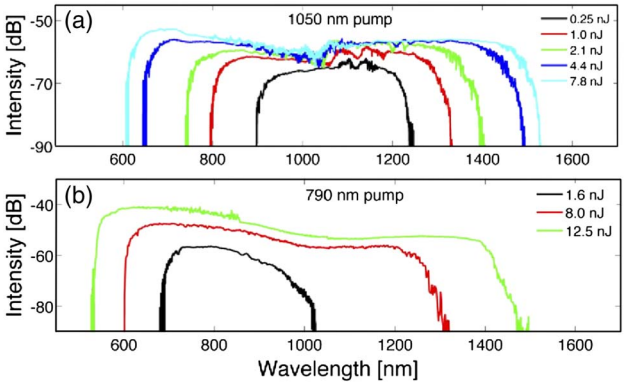

Fig. 7. (Color online) (a) Optical spectra observed at the output of a 50-cm-long PCF when it was pumped at a wavelength of 1050 nm with 50 fs pulses of energies ranging from 0.25 to 7.8 nJ. (b) Output spectra when the same PCF was pumped at 790 nm. (Reproduced with permission [37], ©2011 Optical Society of America.)

D. Applications of Supercontinuum Sources

In recent years, fiber-based supercontinuum sources are being used for a variety of applications, ranging from biomedical imaging to frequency metrology [40]. Such a source can provide an output whose wavelength can be tuned over a range exceeding 1000 nm if a suitable optical filter is placed in front of it. A multiwavelength output can also be obtained if the optical filter has multiple transmission peaks. Such a device is quite useful for wavelength-division multiplexed (WDM) lightwave systems if the wavelengths are uniformly spaced. By 2003, such a technique was used to make a WDM transmitter that delivered 50 GHz spaced optical carriers over a spectral range of 1425–1675 nm [41].

Extreme spectral broadening of femtosecond optical pulses inside a microstructured fiber is useful for any application requiring a broadband source. An obvious example is provided by spectroscopy. Indeed, fiber-based supercontinuum sources have found applications in pump–probe spectroscopy, coherent Raman spectroscopy, near-field optical microscopy, and other forms of coherent nonlinear spectroscopy. These techniques are useful for identifying unknown molecular species as well as for imaging biological samples. A femtosecond spectrometer was built as early as 2002 by using the supercontinuum as a wideband probe [42].

Biomedical imaging can also make use of coherent anti-Stokes Raman scattering microscopy and optical coherence tomography (OCT). Both benefit from fiber-based supercontinuum sources. OCT is capable of providing high-resolution

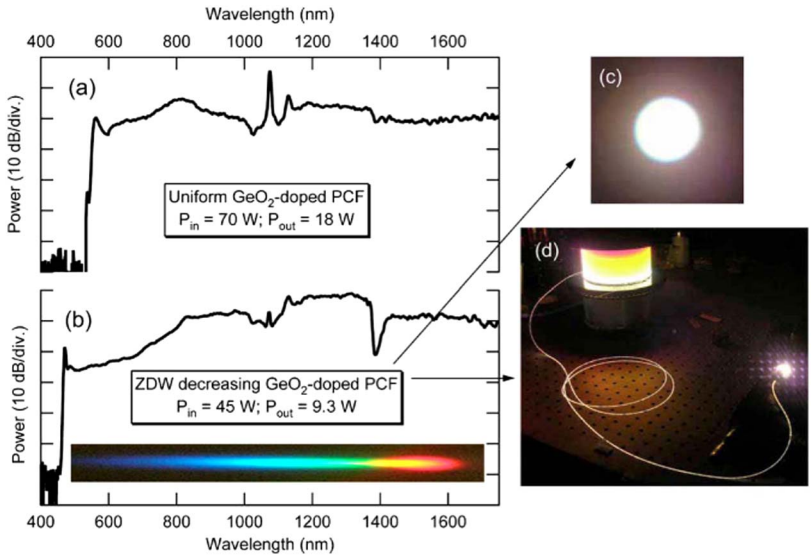

Fig. 8. (Color online) Experimental spectra for a launched power of (a) 70 W in a uniform-core PCF and (b) 45 W in a tapered-core PCF; the inset shows the photograph of output dispersed by a prism. Photographs of (c) the output spot and (d) of the fiber spool are also shown. (Reproduced with permission [39], ©2009 Optical Society of America.)

images of biological tissues even *in vivo*. As early as 2003, a compact light source was used for OCT imaging, in which a pulsed erbium-doped fiber laser was combined with a microstructured fiber to produce a supercontinuum extending from 1100 to 1800 nm [43]. Its use resulted in OCT images with a longitudinal resolution of about 1.4 μm.

A somewhat unexpected application of the supercontinuum occurs in the field of frequency metrology. Precise measurements of optical frequencies are based on a frequency comb (a large number of equally spaced spectral lines) that acts as a ruler. A mode-locked laser can be used for this purpose but it suffers from the problem of carrier-envelope phase mismatch. This problem can be solved if the spectrum extends at least over one octave, and that is where a supercontinuum comes into play. Fiber lasers operating near 1550 nm are employed with PCFs for realizing an all-fiber source of octave-spanning supercontinuum. Such a turn-key, all-fiber system for frequency metrology was demonstrated in 2004 by phase locking the repetition rate and the carrier-envelope offset frequency to a hydrogen maser whose frequency was calibrated with a cesium atomic clock [44].

5. OTHER APPLICATIONS OF NONLINEAR FIBER OPTICS

Because of space limitations, this review has focused mainly on the propagation of short optical pulses as fundamental and higher-order solitons inside optical fibers. The simultaneous presence of nonlinear and dispersive effects leads to a variety of interesting phenomena, supercontinuum generation being the most dramatic example.

When two or more optical waves (CW or pulsed) at different wavelengths are launched inside the fiber simultaneously, several new nonlinear effects become important. Among them, XPM is perhaps the most significant because it occurs irrespective of the wavelength difference among the input waves. It plays a critical role in telecommunication systems in which multiple WDM channels carry information simultaneously over a single optical fiber. XPM can also be used for applications such as photonic switching, wavelength conversion of WDM channels, and optical signal processing. The reader is referred to a recent book for further details on this subject [45].

When the wavelength difference between the two optical signals falls near the dominant peak associated with the Raman gain spectrum (see Fig. 1), the nonlinear phenomenon of SRS can transfer energy from the shorter-wavelength wave (called the pump) to the longer-wavelength wave (called the Stokes). This feature can be used to make Raman amplifiers that amplify a weak optical signal of any wavelength, as long as a pump laser is available whose frequency is upshifted by about 13 THz (see Fig. 1). Such amplifiers are especially useful for fiber-optic WDM systems operating near 1550 nm [46,47]. In this case, the same fiber that is used for data transmission can be employed for Raman amplification. Such a scheme is now commonly used in modern WDM systems for compensating fiber losses [45].

The nonlinear phenomenon of FWM can be exploited for making fiber-optic parametric amplifiers (FOPAs) and oscillators. In the simplest implementation of a FOPA, a weak optical signal is amplified by injecting a pump whose wavelength is detuned from the signal by 10 nm or so and falls close to the zero-dispersion wavelength of the fiber. In this situation, the phase-matching condition can be satisfied if the pump experiences a relatively small amount of anomalous dispersion [19]. With a suitable design, the signal can be amplified by a factor as large as 10,000. Single-pump FOPAs suffer from a limited bandwidth (about 30 nm or so) and from the polarization dependence of the signal gain. These problems can be solved to a large extent by employing two pumps whose wavelengths are widely separated (by 40 nm or more) and fall on the opposite sides of the zero-dispersion wavelength of the fiber [48]. The polarization problem is avoided by polarizing the two pumps orthogonally.

FWM can also occur in the normal-dispersion region provided the fourth-order dispersion parameter is negative at the pump frequency for the fiber employed [19]. This approach has produced FOPAs that can be tuned over a range of several hundred nanometers [49].

The FWM phenomenon also generates a new wave, called the idler wave, at a frequency $\omega_i = 2\omega_p - \omega_s$, where ω_p and ω_s are the pump and signal frequencies, respectively. This frequency relation has its origin in the principle of energy conservation. Physically speaking, FWM converts two pump photons into two new photons at the signal and idler frequencies at a rate that depends on the pump power. The automatic generation of the idler wave inside a FOPA may look like a waste of energy, but it is actually a blessing in disguise since it converts a FOPA into several useful devices. Perhaps the most useful among them is a FWM-based wavelength converter. Modern WDM systems require a device that can convert the wavelength of a channel without affecting its bit pattern (or information content). If an optical filter is placed in front of a FOPA such that it blocks the pump and the signal but lets pass the idler, the output is the original WDM channel at a new wavelength. The bit pattern remains unchanged during the FWM process because an idler pulse is generated only when a signal pulse is present together with the pump. In the case of a wavelength converter, the pump is in the form of a CW wave and its wavelength is chosen at $\omega_p = \frac{1}{2}(\omega_s + \omega_i)$. However, the same device can be used to demultiplex a high-speed bit stream if the pump is in the form of an optical clock (a pulse train) at the frequency at which demultiplexing is performed [40].

Another potential application of FWM is for dispersion compensation in WDM systems [45]. This application rests on the important property of phase conjugation during the FWM process. It turns out that the phase ϕ_i of the idler wave is related to the signal phase ϕ_s by the relation $\phi_i = 2\phi_p - \phi_s + \phi_0$, where ϕ_0 is some constant phase. If the pump phase stays constant during the FWM process, the idler represents the phase conjugate of the signal field. As a result, the sign of the accumulated dispersion is effectively reversed for the idler wave. If phase conjugation is performed in the middle of a fiber-optic link, the dispersion acquired during the first half can be canceled during the second half. Such a scheme has been verified in laboratory demonstrations but has not yet been adopted for commercial systems.

An interesting application of optical fibers uses FWM for producing a source of entangled photon pairs that is useful for applications related to quantum communication, quantum cryptography, and quantum computing. Since the signal and idler photons are generated from the pump photons at the same instant, FWM provides a simple way to generate correlated photon pairs within a single spatial mode. In practice, a pump beam is launched at a wavelength not far from the zero-dispersion wavelength of the fiber such that the phase-matching condition is satisfied for a specific set of signal and idler frequencies. Quantum noise acts as the seed for initiating the so-called spontaneous FWM and generates the correlated signal and idler photons. If it is desirable to have a source that emits correlated photon pairs at the same frequency, a dual-pump configuration is employed in which a nondegenerate FWM process is used to produce the signal and idler photons at the same frequency.

It was observed in several experiments that the quality of the photon-pair source is deteriorated by spontaneous Raman scattering that accompanies the spontaneous FWM process inevitably and cannot be avoided in practice. This problem can be mitigated to a large extent when the signal and idler photons are shifted from the pump frequency by much more than 13 THz to avoid the dominant Raman peak in Fig. 1(a). In a 2005 experiment [50], a 2-m-long PCF was pumped with 4 ps pulses at 708 nm. The FWM condition could be satisfied for the signal and idler photons far from the pump wavelength because pump pulses propagated in the normal-dispersion region of the fiber. Up to 10^7 photon pairs per second were produced at wavelengths of 587 and 897 nm whose quality was not affected much by spontaneous Raman scattering. The resulting device acts as a single-mode source of correlated photon pairs with high brightness. In a 2009 experiment, dispersive properties of short pieces of birefringent PCFs were manipulated to produce photon pairs with no spectral correlations, allowing direct heralding of single photons [51].

6. CONCLUDING REMARKS

It should be evident by now that the field of nonlinear fiber optics has grown substantially from its beginning in the 1970s and has led to the use of optical fibers in unexpected areas. One can only speculate what the future will bring. I mention here a few potential directions. On the fundamental side, optical fibers are playing a key role in the emerging topic of optical rogue waves and its connection to the Peregrine soliton and Akhmediev breathers [52]. It is likely that future studies will advance this topic considerably. On the application side, hollow-core PCFs allow one to fill them with any fluid exhibiting larger nonlinearities than those of glasses. This approach opens up a new area that remains largely unexplored. Finally, glass fibers with a semiconductor core are being developed whose nonlinear properties will enrich the field of nonlinear fiber optics in coming years.

REFERENCES

1. T. H. Maiman, "Stimulated optical radiation in ruby," Nature **187**, 493–494 (1960).
2. P. A. Franken, A. E. Hill, C. W. Peters, and G. Weinreich, "Generation of optical harmonics," Phys. Rev. Lett. **7**, 118–119 (1961).
3. E. J. Woodbury and W. K. Ng, "Ruby laser operation in the near IR," Proc. IRE **50**, 2367 (1962).
4. P. D. Maker, R. W. Terhune, and C. M. Savage, "Intensity-dependent changes in the refractive index of liquids," Phys. Rev. Lett. **12**, 507–509 (1964).
5. R. Y. Chiao, C. H. Townes, and B. P. Stoicheff, "Stimulated Brillouin scattering and coherent generation of intense hypersonic waves," Phys. Rev. Lett. **12**, 592–595 (1964).
6. R. L. Carman, R. Y. Chiao, and P. L. Kelly, "Observation of degenerate stimulated four-photon interaction and four-wave parametric amplification," Phys. Rev. Lett. **17**, 1281–1283 (1966).
7. N. Bloembergen, *Nonlinear Optics* (Benjamin, 1965).
8. F. P. Kapron, D. B. Keck, and R. D. Maurer, "Radiation losses in glass optical waveguides," Appl. Phys. Lett. **17**, 423–425 (1970).
9. R. H. Stolen, E. P. Ippen, and A. R. Tynes, "Raman oscillation in glass optical waveguide," Appl. Phys. Lett. **20**, 62–64 (1972).
10. E. P. Ippen and R. H. Stolen, "Stimulated Brillouin scattering in optical fibers," Appl. Phys. Lett. **21**, 539–541 (1972).
11. R. H. Stolen and A. Ashkin, "Optical Kerr effect in glass waveguide," Appl. Phys. Lett. **22**, 294–296 (1973).
12. R. H. Stolen, J. E. Bjorkholm, and A. Ashkin, "Phase-matched three-wave mixing in silica fiber optical waveguides," Appl. Phys. Lett. **24**, 308–310 (1974).
13. R. H. Stolen, "Phase-matched-stimulated four-photon mixing in silica-fiber waveguides," IEEE J. Quantum Electron. **11**, 100–103 (1975).
14. R. H. Stolen and C. Lin, "Self-phase-modulation in silica optical fibers," Phys. Rev. A **17**, 1448–1453 (1978).

15. A. Hasegawa and F. Tappert, "Transmission of stationary nonlinear optical pulses in dispersive dielectric fibers: I. Anomalous dispersion," Appl. Phys. Lett. **23**, 142–144 (1973).
16. L. F. Mollenauer, R. H. Stolen, and J. P. Gordon, "Experimental observation of picosecond pulse narrowing and solitons in optical fibers," Phys. Rev. Lett. **45**, 1095–1098 (1980).
17. L. F. Mollenauer and R. H. Stolen, "The soliton laser," Opt. Lett. **9**, 13–15 (1984).
18. R. H. Stolen, "The early years of fiber nonlinear optics," J. Lightwave Technol. **26**, 1021–1031 (2008).
19. G. P. Agrawal, *Nonlinear Fiber Optics*, 4th ed. (Academic, 2007).
20. R. W. Boyd, *Nonlinear Optics*, 3rd ed. (Academic, 2008).
21. E. P. Ippen, in *Laser Applications to Optics and Spectroscopy*, S. F. Jacobs, M. Sargent III, J. F. Scott, and M. O. Scully, eds. (Addison-Wesley, 1975), Vol. 2, Chap. 6.
22. R. H. Stolen, J. P. Gordon, W. J. Tomlinson, and H. A. Haus, "Raman response function of silica-core fibers," J. Opt. Soc. Am. B **6**, 1159–1166 (1989).
23. Q. Lin and G. P. Agrawal, "Raman response function for silica fibers," Opt. Lett. **31**, 3086–3088 (2006).
24. P. K. A. Wai, C. R. Menyuk, Y. C. Lee, and H. H. Chen, "Nonlinear pulse propagation in the neighborhood of the zero-dispersion wavelength of monomode optical fibers," Opt. Lett. **11**, 464–488 (1986).
25. Y. Kodama and A. Hasegawa, "Nonlinear pulse propagation in a monomode dielectric guide," IEEE J. Quantum Electron. **23**, 510–524 (1987).
26. P. Beaud, W. Hodel, B. Zysset, and H. P. Weber, "Ultrashort pulse propagation, pulse breakup, and fundamental soliton formation in a single-mode optical fiber," IEEE J. Quantum Electron. **23**, 1938–1946 (1987).
27. K. Tai, A. Hasegawa, and N. Bekki, "Fission of optical solitons induced by stimulated Raman effect," Opt. Lett. **13**, 392–394 (1988).
28. N. Akhmediev and M. Karlsson, "Cherenkov radiation emitted by solitons in optical fibers," Phys. Rev. A **51**, 2602–2607 (1995).
29. F. M. Mitschke and L. F. Mollenauer, "Discovery of the soliton self-frequency shift," Opt. Lett. **11**, 659–661 (1986).
30. J. P. Gordon, "Theory of the soliton self-frequency shift," Opt. Lett. **11**, 662–664 (1986).
31. J. Santhanam and G. P. Agrawal, "Raman-induced spectral shifts in optical fibers: general theory based on the moment method," Opt. Commun. **222**, 413–420 (2003).
32. X. Liu, C. Xu, W. H. Knox, J. K. Chandalia, B. J. Eggleton, S. G. Kosinski, and R. S. Windeler, "Soliton self-frequency shift in a short tapered air–silica microstructure fiber," Opt. Lett. **26**, 358–360 (2001).
33. J. K. Ranka, R. S. Windeler, and A. J. Stentz, Opt. Lett. **25**, 25–27 (2000).
34. J. M. Dudley, G. Genty, and S. Coen, "Supercontinuum generation in photonic crystal fiber," Rev. Mod. Phys. **78**, 1135–1184 (2006).
35. G. Qin, X. Yan, C. Kito, M. Liao, C. Chaudhari, T. Suzuki, and Y. Ohishi, "Ultrabroadband supercontinuum generation from ultraviolet to 6.28 μm in a fluoride fiber," Appl. Phys. Lett. **95**, 161103 (2009).
36. J. M. Dudley and J. R. Taylor, eds., *Supercontinuum Generation in Optical Fibers* (Cambridge University, 2010).
37. A. M. Heidt, A. Hartung, G. W. Bosman, P. Krok, E. G. Rohwer, H. Schwoerer, and H. Bartelt, "Coherent octave spanning near-infrared and visible supercontinuum generation in all-normal dispersion photonic crystal fibers," Opt. Express **19**, 3775–3787 (2011).
38. J. C. Travers, "Continuous wave supercontinuum generation," in *Supercontinuum Generation in Optical Fibers* (Cambridge University, 2010), Chap. 8.
39. A. Kudlinski, G. Bouwmans, O. Vanvincq, Y. Quiquempois, A. Le Rouge, L. Bigot, G. Méelin, and A. Mussot, "White-light cw-pumped supercontinuum generation in highly GeO_2-doped core photonic crystal fibers," Opt. Lett. **34**, 3631–3634 (2009).
40. G. P. Agrawal, *Applications of Nonlinear Fiber Optics*, 2nd ed. (Academic, 2008).
41. K. Mori, K. Sato, H. Takara, and T. Ohara, "Supercontinuum lightwave source generating 50 GHz spaced optical ITU grid seamlessly over S-, C- and L-bands," Electron. Lett. **39**, 544–546 (2003).
42. V. Nagarajan, E. Johnson, P. Schellenberg, W. Parson, and R. Windeler, "A compact versatile femtosecond spectrometer," Rev. Sci. Instrum. **73**, 4145–4149 (2002).
43. K. Bizheva, B. Povazay, B. Hermann, H. Sattmann, W. Drexler, M. Mei, R. Holzwarth, T. Hoelzenbein, V. Wacheck, and H. Pehamberger, "Compact, broad-bandwidth fiber laser for sub-2-μm axial resolution optical coherence tomography in the 1300 nm wavelength region," Opt. Lett. **28**, 707–709 (2003).
44. T. R. Schibli, K. Minoshima, F.-L. Hong, H. Inaba, A. Onae, H. Matsumoto, I. Hartl, and M. E. Ferman, "Frequency metrology with a turnkey all-fiber system," Opt. Lett. **29**, 2467–2469 (2004).
45. G. P. Agrawal, *Fiber-Optic Communication Systems*, 4th ed. (Wiley, 2010).
46. M. N. Islam, ed., *Raman Amplifiers for Telecommunications* (Springer, 2003), Parts 1 and 2.
47. C. Headley and G. P. Agrawal, eds. *Raman Amplification in Fiber Optical Communication Systems* (Academic, 2005).
48. M. E. Marhic, *Fiber Optical Parametric Amplifiers, Oscillators and Related Devices* (Cambridge University, 2007).
49. Y. Deng, Q. Lin, F. Lu, G. P. Agrawal, and W. H. Knox, "Broadly tunable femtosecond parametric oscillator using a photonic crystal fiber," Opt. Lett. **30**, 1234–1236 (2005).
50. J. Fulconis, O. Alibart, W. J. Wadsworth, P. St. J. Russell, and J. G. Rarity, "High brightness single mode source of correlated photon pairs using a photonic crystal fiber," Opt. Express **13**, 7572–7582 (2005).
51. O. Cohen, J. S. Lundeen, B. J. Smith, G. Puentes, P. J. Mosley, and I. A. Walmsley, "Tailored photon-pair generation in optical fibers," Phys. Rev. Lett. **102**, 123603 (2009).
52. B. Kibler, J. Fatome, C. Finot, G. Millot, F. Dias, G. Genty, N. Akhmediev, and J. M. Dudley, "The Peregrine soliton in nonlinear fibre optics," Nat. Phys. **6**, 790–795 (2010).